



HHS Public Access

Author manuscript

Biomaterials. Author manuscript; available in PMC 2016 May 01.

Published in final edited form as:

Biomaterials. 2015 May ; 51: 208–215. doi:10.1016/j.biomaterials.2015.02.015.

Nanoparticle formulations of histone deacetylase inhibitors for effective chemoradiotherapy in solid tumors

Edina C. Wang^{1,†,§}, Yuanzeng Min^{1,†,§}, Robert C. Palm^{†,§}, James J. Fiordalisi[†], Kyle T. Wagner^{†,§}, Nabeel Hyder^{†,§}, Adrienne D. Cox[†], Joseph Caster[†], Xi Tian^{†,§}, and Andrew Z. Wang^{†,§,*}

[§]Laboratory of Nano- and Translational Medicine, Lineberger Comprehensive Cancer Center, Carolina Center for Cancer Nanotechnology Excellence, Carolina Institute of Nanomedicine, University of North Carolina at Chapel Hill, Chapel Hill, NC 27599, USA

[†]Department of Radiation Oncology, Lineberger Comprehensive Cancer Center, Carolina Center for Cancer Nanotechnology Excellence, Carolina Institute of Nanomedicine, University of North Carolina at Chapel Hill, Chapel Hill, NC 27599, USA

Abstract

Histone deacetylase inhibitors (HDACIs) represent a class of promising agents that can improve radiotherapy in cancer treatment. However, the full therapeutic potential of HDACIs as radiosensitizers has been restricted by limited efficacy in solid malignancies. In this study, we report the development of nanoparticle (NP) formulations of HDACIs that overcome these limitations, illustrating their utility to improve the therapeutic ratio of the clinically established first generation HDACI vorinostat and a novel second generation HDACI quisinostat. We demonstrate that NP HDACIs are potent radiosensitizers *in vitro* and are more effective as radiosensitizers than small molecule HDACIs *in vivo* using mouse xenograft models of colorectal and prostate carcinomas. We found that NP HDACIs enhance the response of tumor cells to radiation through the prolongation of γ -H2AX foci. Our work illustrates an effective method for improving cancer radiotherapy treatment.

Keywords

Nanoparticle; Drug delivery; Chemotherapy; Controlled drug release

© 2015 Published by Elsevier Ltd.

This manuscript version is made available under the CC BY-NC-ND 4.0 license.

*Corresponding Author: Andrew Z. Wang, (P) 919-966-7700, (F) 919-966-7681, zawang@med.unc.edu.

[†]These authors contributed equally to this work

Publisher's Disclaimer: This is a PDF file of an unedited manuscript that has been accepted for publication. As a service to our customers we are providing this early version of the manuscript. The manuscript will undergo copyediting, typesetting, and review of the resulting proof before it is published in its final citable form. Please note that during the production process errors may be discovered which could affect the content, and all legal disclaimers that apply to the journal pertain.

INTRODUCTION

Histone deacetylases (HDACs) are enzymes involved in the regulation of gene expression and chromatin modification [1]. Aberrant activity of HDACs has been implicated in cancer development. Consequently, the inhibition of HDACs has emerged as a promising strategy to reverse aberrant epigenetic states associated with cancer [2]. There has been extensive development of histone deacetylase inhibitors (HDACIs) as a new class of therapeutics for both solid tumors and hematologic malignancies. Unfortunately, these efforts have only resulted in approval of HDACIs (vorinostat (suberoylanilide hydroxamic acid, SAHA) and romidepsin (depsipeptide)) for the treatment of cutaneous T-cell lymphoma [3, 4]. In the clinic, HDACIs have not significantly improved outcomes in solid malignancies compared with current standard therapies [2]. One of the potential clinical applications of HDACIs is to improve radiotherapy treatment, a treatment that more than 60% of all cancer patients will receive [5]. Preclinical studies have indicated that a number of HDAC inhibitors are effective radiosensitizers [6], agents that sensitize tumor cells to radiotherapy, in a variety of solid malignancies such as colorectal cancer [7] and prostate cancer cells [8]. However, the radiosensitization effects have been associated with only mild improvements in efficacy. Given the promise of HDACIs as radiosensitizers, the identification of strategies to improve their therapeutic ratio is needed.

The specific mechanisms by which HDACIs induce radiosensitization remains unresolved, but may be due in part to the prevention of the DNA double strand (DSB) repair, the principal mechanism of action of radiotherapy, leading to subsequent tumor cell death [6, 9]. HDACIs have been shown to prolong the formation of phosphorylated histone H2AX (γ H2AX), a marker of DSBs, following radiation [9-11]. HDACIs may promote the stabilization of DNA DSBs through a variety of mechanisms including the downregulation of specific DNA repair molecules such as Ku70, Ku86, Rad50 and Rad51 [6, 12]. HDAC inhibition may also lead to hyperacetylation of histones, leading to a more relaxed chromatin state [1]. This may enhance exposure of DNA to radiation-induced damage.

It has been postulated that the efficacy of established first-generation HDACIs were limited in solid tumor indications due to their suboptimal potency for specific HDAC enzymes and transient induction of histone acetylation in tumor tissue [13]. In agreement with this notion, it has been shown that prolonged exposure of HDACI vorinostat is necessary for tumor growth inhibition. Furthermore, vorinostat's inhibitory activity is rapidly reversible upon removal of the drug [14]. This may explain the limited efficacy of vorinostat in combination with radiotherapy in solid malignancies. Thus, more potent second-generation HDACIs, such as quisinostat (JNJ-26481585) have been developed with the goal to prolong pharmacodynamic response and to increase efficacy [13]. Quisinostat have been shown to exert antiproliferative activity against a wide panel of cancer cell lines at nanomolar concentrations. The potent and prolonged activity of quisinostat is found to translate into higher *in vivo* potency in preclinical colorectal cancer tumor models than vorinostat. However, more potent HDACIs can also be associated with increased toxicity to normal tissues [15].

Therefore, there are two key limitations in the current use of HDACIs as radiosensitizers. First, clinically established HDACIs may be inefficient at sustaining inhibition of DSB repair, leading to limited efficacy in improving radiotherapy. Second, more potent HDACIs may sensitize both tumor and normal cells to the effects of radiotherapy, leading to increased toxicity. Thus, there is strong interest in the development of novel strategies to further improve their therapeutic ratio in chemoradiotherapy. One approach is to utilize nanoparticle (NP) drug delivery vehicles. NPs preferentially accumulate in tumors and have low distribution in normal tissue [16, 17]. They can also release HDACIs in a slow and controlled fashion to further increase synergy with radiotherapy (Fig. 1b). We hypothesized that NP formulations of HDACIs will lead to higher therapeutic ratio when combined with radiotherapy than small molecule HDACIs. In this study, we engineered biodegradable and biocompatible NP formulations of first generation HDACI vorinostat and second generation HDACI quisinostat. These NP HDACIs were evaluated as radiosensitizers *in vitro* using two prostate and three colorectal cancer cell lines. The *in vitro* data was further validated *in vivo* using mouse xenograft models of prostate and colorectal cancers.

MATERIALS AND METHODS

Materials

Vorinostat was purchased from Biotang Inc (Boston, MA, USA). Quisinostat was obtained from Active Biochem (Maplewood, NJ, USA). Poly (D,L-lactide-coglycolide) (PLGA) with a 85:15 monomer ratio, ester terminated, and viscosity of 0.55-0.75 dL/g was purchased from Durect Corporation (Pelham, AL, USA). PLGA with a 50:50 monomer ratio, ester terminated, and viscosity of 0.72–0.92 dl/g was purchased from Durect Corporation (Pelham, AL). Soybean lecithin consisting of 90-95% (w/w) phosphatidylcholine was obtained from MP Biomedicals (Solon, OH, USA). DSPE-PEG2000-COOH [1,2-distearoyl-sn-glycero-3-phosphoethanolamine-N-carboxy (polyethylene glycol) 2000] was purchased from Avanti Polar Lipids (Alabaster, AL, USA).

Characterization of nanoparticle vorinostat and nanoparticle quisinostat

NP vorinostat and NP quisinostat size (diameter, nm) and surface charge (ζ -potential, mV) were characterized using a Zetasizer Nano Z dynamic light scattering detector (Malvern Instruments, Westborough, MA, USA). Transmission electron microscopy (TEM) images of NP vorinostat and NP quisinostat were obtained at the Microscopy Services Laboratory Core Facility at the UNC School of Medicine.

Synthesis and characterization of nanoparticle vorinostat and nanoparticle quisinostat

PLGA-lecithin-PEG core-shell NPs were synthesized from PLGA, soybean lecithin, and DSPE-PEG-COOH using a modified nanoprecipitation technique[18]. Vorinostat and quisinostat was dissolved at a dosage of 10% (w/w) of the polymer into the PLGA/ acetonitrile solution before nanoprecipitation. The NP solution was washed twice using an Amicon Ultra-4 centrifugal filter (Millipore, MA, USA) with a molecular weight cutoff of 30 kDa and then resuspended in PBS to obtain the final concentration. NP vorinostat and NP quisinostat size (diameter, nm) and surface charge (ζ -potential, mV) were characterized

using a Zetasizer Nano Z dynamic light scattering detector (Malvern Instruments Ltd, Worcestershire, UK).

Nanoparticle vorinostat and nanoparticle quisinostat release

To measure the release profile of vorinostat from NP vorinostat and quisinostat from NP quisinostat, 400 μ L of NP vorinostat or NP quisinostat solution at a concentration of 1 mg/mL was aliquot equally into Slide-A-Lyzer MINI dialysis microtubes with a molecular weight cut-off of 2 kDa (Pierce, Rockford, IL, USA) and subjected to dialysis against 4 L of phosphate-buffered saline (PBS) with gentle stirring at 37°C. PBS was changed periodically during the dialysis process. At the indicated times, 0.1 mL of solution from three microtubes was removed and mixed with an equal volume of acetonitrile to dissolve the NPs. Vorinostat and quisinostat content from their respective NPs were quantitatively analyzed using an Agilent 1100 HPLC (Palo Alto, CA, USA) equipped with a C18 chromolith flash column (Merck KGaA Darmstadt, Germany). Vorinostat absorbance was measured by a UV-VIS detector at 228 nm and in 0.25 mL/min gradient (from 0:100 to 100:0) of acetonitrile/water. Quisinostat absorbance was measured by a UV-VIS detector at 228 nm and in 0.25 mL/min gradient (from 0:100 to 100:0) of methanol: water with 0.1% TFA.

Cell culture

DU145, PC3, HCT116, and SW620 cells were acquired from the Tissue Culture Facility at the Lineberger Comprehensive Cancer Center at UNC. DU145 cells were cultured in EMEM supplemented with 10% fetal bovine serum (FBS) (Mediatech, Manassas, VA, USA), nonessential amino acids (Mediatech), and penicillin/streptomycin (Mediatech), and sodium pyruvate (Gibco). PC3 cells were cultured in DMEM/F12 (Gibco) supplemented with 10% FBS and penicillin/streptomycin (Mediatech). HCT116 cells was cultured in McCoy's 5A with L-glutamine (Mediatech) supplemented with 10% FBS and penicillin/streptomycin (Mediatech). SW620 cells was cultured in DMEM-H (Gibco, Invitrogen, Carlsbad, CA, USA) supplemented with 10% FBS (Mediatech) and penicillin/streptomycin (Mediatech). SW837 (ATCC™ CCL-235™) (ATCC, Manassas, VA, USA) cells were maintained in DMEM-H (Gibco, Invitrogen, Carlsbad, CA, USA) supplemented with 10% FBS (Mediatech) and penicillin/streptomycin (Mediatech).

Clonogenic survival assay

Cells were treated with 1 μ M of vorinostat or 1 μ M quisinostat either without NPs or encapsulated in NPs for 24 h. Cells were washed 2 times with phosphate buffer saline (PBS) after incubation. Cells were then seeded at various densities ranging from 100 to 50,000 cells in 4 mL of culture medium in 50 mL flasks following treatment. The cells were then irradiated at 0, 2, 4, 6 or 8 Gy. Radiotherapy was given using a Precision X-RAD 320 (Precision X-Ray, Inc., North Branford, CT) machine operating at 320 kVp and 12.5mA. The dose rate at a source-subject distance of 50 cm was 2.07 Gy/min. The cells were incubated for 10 days following irradiation. After 10 days, the cells were fixed in 1:1 acetone/methanol and were stained with trypan blue. Colonies with over 50 cells were counted. The relative survival fraction was calculated by dividing the number of colonies of irradiated cells by the number of cells plated, with correction for the plating efficiency. The average plating efficiency (%) for PC3, DU145, HCT116, SW620, and SW837 cells were 52, 40, 66, 66,

and 29 respectively. Survival fractions significantly lower than 0.001 were excluded from analysis.

Immunofluorescent Staining for γ -H2AX

1×10^5 PC3 cells were grown in a 24-well plate and treated with $1 \mu\text{M}$ small molecule vorinostat equivalent of NP vorinostat or vorinostat. Cells were incubated for 24 hr and then washed in PBS thrice and incubated with fresh medium. The cells were then treated with 2 Gy using a Precision XRAD 320. At specified times, medium was aspirated and cells were fixed in 4% paraformaldehyde for 15 minutes at room temperature. Paraformaldehyde was aspirated and the cells were then washed in PBS thrice, permeabilized with 0.5% Triton X-100 followed by PBS wash thrice. Cells were then blocked with 5% bovine serum albumin in PBS for 1 h, following which mouse monoclonal anti- γ -H2AX antibody (Millipore) was added at a dilution of 1:200 in 1% bovine serum albumin in PBS and incubated for 1 h at room temperature. Cells were then washed thrice in PBS before incubating in the dark with donkey anti-mouse Alexa Fluor 594 (Invitrogen) at a dilution of 1:1000 in 1% bovine serum albumin in PBS for 1 h. The secondary antibody solution was then aspirated and the cells were washed three times in PBS. Cells were then examined using a Leica confocal microscope.

Tumor efficacy

PC3 or SW620 cells (1×10^6 cells in 200 μL 1:1 RPMI-1640 and matrigel) were injected s.c. into the left flank of 6-8 week-old male Nu/Nu mice to develop xenograft tumors. Ten days after inoculation, the mice were randomly distributed into different groups for subsequent treatment. Saline, vorinostat, NP vorinostat, was tail vein i.v. injected at an equivalent dose of 0.93 mg/kg vorinostat. Quisinostat or NP quisinostat was tail vein i.v. injected at an equivalent dose of 1.33 mg/kg quisinostat. Three hours post-injection, the tumors were subjected to a dose of 3 Gy with Precision XRAD 320. The mice were covered with a lead shield to allow irradiation of the tumor site and minimal irradiation to other organs. Tumor volumes were measured every 2 days by measuring two perpendicular diameters with a caliper. The tumor volume was calculated with the formula $V = 0.5 \times a \times b^2$ where a is the larger diameter and b is the smaller diameter. The relative change in tumor volume was calculated using the relation V_i/V_0 , where V_i is the volume on measured day and V_0 is the initial volume on day 0. Animals were monitored in accordance to the guidelines presented in the University of North Carolina Institutional Animal Care and Use Committee approved protocol for this study. For statistical analysis, we calculated the area under the growth curve (AUC). On the basis of the AUCs, the Wilcoxon rank sum test was performed to compare the growth rates between the two groups. The exact one-sided p -value of the Wilcoxon rank sum test was calculated. Data were considered statistically significant when the p value was less than 0.05.

RESULTS

In this study, we synthesized NP formulations of two HDACIs: established first generation HDACI vorinostat and novel second generation HDACI quisinostat. Lipid-polymer NPs were prepared using a modified nanoprecipitation method [18]. Vorinostat and quisinostat

are hydrophobic molecules, which allowed for NP encapsulation. We investigated two forms of PLGA polymers: ester- and carboxyl-terminated PLGA. We also studied PLGA with different percentages of lactide and glycolide moieties (e.g. 50:50 and 85:15 PLGA) since polymer composition can determine the degradation rate of the lipid-polymer NP carrier, which in turn affects the drug release rate [19]. The effects of the investigated parameters on NP formation are summarized in Table S1-S2.

We found that NP formulations of vorinostat synthesized with ester-terminated PLGA with a lactide and glycolide ratio of 85:15 were more compact in size and monodisperse compared with NPs formulated with either ester or acid-terminated 50:50 PLGA (Table S1). In general, NPs with sizes below 200 nm preferentially accumulate in tumor tissues *via* the enhanced permeability and retention (EPR) effect [20]. NP quisinostat synthesized with either acid or ester-terminated 50:50 PLGA did not form particles with sizes suitable for tumor uptake (Table S1). In contrast, NP quisinostat synthesized with 85:15 PLGA possess sizes of 125.7 ± 2.4 nm. The end-group functionalization of PLGA also affected particle size and polydispersity. We found that NP vorinostat formulated with carboxyl-terminated 50:50 PLGA possess smaller sizes and was more monodisperse than NP vorinostat synthesized with ester-terminated 50:50 PLGA. Furthermore, NP vorinostat synthesized with ester-terminated 85:15 PLGA was both smaller in size and had higher drug loading than NPs formulated with carboxyl-terminated 50:50 PLGA (Table S2).

Therefore, for the following studies, we formulated lipid-polymer NP vorinostat and NP quisinostat with 85:15 ester-terminated PLGA (Fig. 1a). The loading attained was 2.2% of vorinostat by weight and 2.3% of quisinostat by weight. As shown in Figure 2a, both NP vorinostat and NP quisinostat demonstrated consistent spherical morphologies on TEM. Dynamic Light Scattering (DLS) analysis showed that NP vorinostat possess sizes of 72.6 ± 3.6 nm, surface charges (ζ potential) of -38.4 ± 2.6 mV and a polydispersity of 0.07 ± 0.01 . NP quisinostat was found to possess sizes of 125.7 ± 2.4 nm and ζ potential of -17.5 ± 3.1 mV. The monodisperse NPs had a polydispersity index of 0.06 ± 0.01 .

Next, we characterized the drug release kinetics of vorinostat and quisinostat from the NPs. Drug release studies were conducted by dialyzing NPs containing vorinostat or quisinostat against 4 L of PBS at pH 7.4 and 37°C to mimic physiological conditions. High-performance liquid chromatography (HPLC) confirmed the release of intact vorinostat or quisinostat from the NPs. Drug delivery carriers formed from PLGA with a higher content of lactide to glycolide moieties (e.g. 85:15 PLGA) are less hydrophilic and thus degrade slower than NPs engineered with higher glycolic acid content [19]. Thus, we theorized that our NP formulations of the HDACIs will have a slow release profile. As shown in Figure 2b, NP vorinostat releases its cargo in a controlled fashion over 4 days, with >95% drug release thereafter. The release of NP quisinostat also demonstrated slow, controlled drug release kinetics with 95% of the drug released from the NP at 4 days (Fig. 2b). These results suggest that our designed NPs enable sustained release of HDACIs. Such prolonged drug release can cause increased synergistic effects between NP HDACIs and radiotherapy, resulting in improved therapeutic efficacy. In the following set of experiments, we evaluated NP HDACIs as radiosensitizers *in vitro* in five tumor cell lines representing three different carcinomas: HCT116 (colon cancer), SW620 (colon cancer), SW837 (rectal cancer), PC3

(prostate cancer) and DU145 (prostate cancer). We conducted radiosensitization experiments using 1 μ M concentration of NP vorinostat, NP quisinostat, vorinostat or quisinostat at small molecule equivalent dose with radiotherapy occurring 24 h following HDACI treatment. The surviving fractions were determined at each radiotherapy dose level. As shown in the clonogenic survival curves depicted in Figure 3, NP vorinostat is more effective than small molecule vorinostat in PC3, DU145, HCT116, and SW837 cell lines at 6 Gy and is nearly as effective as small molecule vorinostat in SW620 cells. We found that NP quisinostat is also an effective radiosensitizer in the five cell lines (Fig. 3). Both NP vorinostat and NP quisinostat increased the sensitivity of various solid tumor cell lines to radiotherapy (Table S3). Specifically, the sensitizer enhancement ratio (SER) of vorinostat at 10% survival in DU145 cells is 1.26, whereas the SER of NP vorinostat is 1.27. The SER of NP vorinostat at 10% is also greater in HCT116 cells with NP vorinostat at 1.71 and vorinostat at 1.48. In SW837 cells, the SER of NP vorinostat at 10% survival is greater at 1.19 compared to vorinostat at 1.08. In SW620 cells, the SER of quisinostat at 10% survival is 1.18 with NP quisinostat at 1.23. Similarly, the SER for NP quisinostat at 10% is greater in SW837 cells with NP quisinostat at 1.15 and quisinostat at 1.00. These results suggest that NP formulations of HDACIs are potent radiosensitizers.

HDACIs are proposed to sensitize tumor cells to radiotherapy partly through the inhibition of DNA damage repair. To compare the relative potency of NP formulation of HDACI and their small molecule counterpart to inhibit DNA damage repair, we evaluated the effect of NP vorinostat and vorinostat on γ H2AX foci, an indicator of DNA DSBs, by immunofluorescence microscopy. PC3 tumor cells were treated with 1 μ M concentration of vorinostat or NP vorinostat at small molecule equivalent dose followed by radiotherapy (2 Gy). The average number of γ H2AX foci per cell was counted and the results are shown in Figure 4. Cells treated with vorinostat plus radiotherapy or NP vorinostat plus radiotherapy produced a greater number of γ H2AX foci compared to cells treated with radiotherapy alone (Fig. S1, Fig. 4). In both vorinostat and NP vorinostat-treated cells, radiation-induced γ H2AX foci were present and the complexes persisted for the duration of the culture (Fig. 4). The prolongation of γ H2AX foci suggests that NP vorinostat has similar inhibitory effects as vorinostat against the repair of DNA damage. We observed that treatment with NP vorinostat alone had a slight effect on γ H2AX foci compared with vorinostat alone. Treatment with NP vorinostat also resulted in a higher number of radiotherapy-induced γ H2AX foci compared to vorinostat. Specifically, a marked increase in γ H2AX foci was seen in NP vorinostat-treated cells 12 and 24 hours post-radiotherapy compared with cells treated with small molecule vorinostat. These results indicate that NP vorinostat is more effective than small molecule vorinostat in increasing the inhibition of DNA DSB repair post-radiotherapy. Generally, the persistence of DNA damage can also lead to increased tumor cell death.

To confirm our *in vitro* findings that NP HDACIs are effective radiosensitizers, we evaluated the therapeutic efficacy of NP vorinostat as a radiosensitizer using a murine xenograft model of cancer. Mice bearing PC3 flank xenograft tumors were treated with saline, vorinostat or NP vorinostat followed by a single dose of radiotherapy. Tumor volumes were measured and tumor growth delay curves were generated (Fig. 5). We

observed a significant difference in tumor growth delay between small molecule vorinostat and NP formulation of vorinostat with the latter being more effective (Fig. 5a). The difference between saline and vorinostat plus radiotherapy does not appear significant ($p = 0.05$). When the tumor growth delay curves were compared between mice receiving saline and NP vorinostat, the difference in delay was found to be statistically significant ($p < 0.01$). We also investigated the therapeutic efficacy of NP quisinostat as a radiosensitizer *in vivo*. Mice bearing subcutaneous flank xenografts of SW620 cells were administered saline, quisinostat only, NP quisinostat only, quisinostat followed by a single dose of radiotherapy or NP quisinostat followed by a single dose of radiotherapy (Fig. 5b, Fig. S2). The difference between saline and quisinostat plus radiotherapy does not appear significant in SW620 cells ($p = 0.22$) although the trend is consistent with such observation (Fig. 5b). In contrast, NP quisinostat plus radiotherapy was found to be more effective than saline or radiotherapy only (Fig. 5b). These results indicate that NP formulation of HDACIs markedly increases the efficacy of HDACIs as radiosensitizers in colorectal and prostate carcinomas. Our *in vivo* data demonstrate the potential of NP HDACIs in improving chemoradiotherapy.

DISCUSSION

HDACIs represent a class of therapeutics that have considerable potential in targeting epigenetic aberrations associated with cancer growth and development [1]. A variety of HDACIs are being assessed in both hematological and solid malignancies. However, in the clinic, HDACIs as a monotherapy have shown limited success in solid tumor indications. Consequently, there has been extensive interest in using HDACIs in combination with other anti-cancer agents such as radiotherapy to increase therapeutic efficacy [21]. The limited efficacy of some HDACIs is due in part to pharmacologic parameters such low bioavailability and short circulating half-lives that prevent prolonged drug exposure. Vorinostat, one of the two HDACIs currently approved in the clinic, has a bioavailability of 43% and a half-life of approximately 2.0 h [22]. As a result of these limitations, novel HDACIs such as quisinostat have been designed to be more potent [13]. On the other hand, these HDACIs also incur increased toxicity to normal tissues. The present studies, using NP formulations of vorinostat and quisinostat, were therefore performed to improve the therapeutic efficacy of HDACI-based chemoradiotherapy. To our knowledge, there have been no published reports of drug delivery vehicles that improve the therapeutic index of HDACIs.

We reported the synthesis of lipid-polymer NPs for the delivery of HDACIs for chemoradiotherapy. The optimization of NP HDACIs was investigated since the physical characteristics of the NPs can play an important role in the exposure of drug to cells and drug half-life in systemic circulation [23]. In this study, we analyzed the effects of different PLGA copolymer ratios and found NPs formed from PLGA with increased lactic acid to glycolic acid improves HDACI loading and lead to more compact particles. We found that NP HDACIs formulated with 85:15 ester-terminated PLGA are monodisperse particles with sizes approximately 72.6 nm for NP vorinostat and 125.6 nm for NP quisinostat. We demonstrated that both NP vorinostat and NP quisinostat release their cargo in a slow and controlled fashion, with approximately 50% drug release after 24 hours and >95% of drug

release after 4 days. Such slow drug release can increase the drug exposure time, which can lead to increased synergistic activity between the HDACIs and radiotherapy in tumor cells.

Our study compared the therapeutic ratio of NP HDACIs as radiosensitizers to that of small molecule HDACIs. We demonstrated that NP vorinostat and NP quisinostat were effective radiosensitizers *in vitro* in colorectal and prostate carcinomas. Previous investigations have demonstrated that at sites of DNA DSBs, the histone H2AX becomes phosphorylated (γ -H2AX), forming complexes indicating DNA damage [11]. To evaluate the involvement of DNA repair in NP vorinostat-mediated radiosensitization, we tested whether NP vorinostat causes a prolongation of γ -H2AX foci, which would suggest a decrease in the rate of repair of radiotherapy-induced DNA damage. Our results showed that the number of γ -H2AX foci is higher in tumor cells treated with NP vorinostat plus radiotherapy compared with cells treated with vorinostat plus radiotherapy. This effect is evident at times up to 24 hours following irradiation. Thus, the increased number of γ -H2AX foci in NP vorinostat-treated cells may be an indicator that NP vorinostat is a more effective inhibitor of the DSB repair pathway than small molecule vorinostat. The ability of NP HDACIs to prolong DNA damage repair inhibition can lead to increased cell death.

We also demonstrated that at equivalent doses of small molecule HDACIs, NP HDACIs are more effective than their small molecule counterparts in chemoradiotherapy *in vivo*. NP vorinostat was capable of marked tumor growth inhibition in a synergistic manner for over 60 days after administration of a single irradiation dose of 3 Gy. We also showed that NP formulation of quisinostat improved its therapeutic efficacy. These results confirmed our hypothesis that NP formulations of HDACIs can significantly improve chemoradiotherapy. NP therapeutics offer several advantages in chemoradiotherapy including controlled drug release and unique biodistribution. Only the effects of controlled drug release were observed *in vitro*. NP HDACIs were found to be more effective than their small molecule counterparts in some cell lines. In other cell lines, the SERs of small molecule HDACIs at 10% survival were higher than the SERs of their NP counterparts. This effect was observed with vorinostat and NP vorinostat in PC3 cells. However, the *in vivo* tumor growth delay curves demonstrated that NP vorinostat lead to a significantly longer tumor growth delay compared with vorinostat in PC3 cells. In the *in vivo* setting, it is likely then that the significant differences in the therapeutic efficacy between small molecule HDACIs and NP HDACIs are due to the unique biodistribution of the NP therapeutics. Presumably, NP HDACIs are able to accumulate in tumors more than small molecule HDACIs and release their cargo in a slow and controlled fashion. This may allow the NPs to exert a greater therapeutic effect, leading to a synergistic interaction between the NP HDACIs and radiotherapy.

CONCLUSIONS

In summary, we have synthesized novel NP formulations of HDACIs vorinostat and quisinostat. The NP HDACIs are compact in size and release drug in a slow and controlled fashion. NP HDACIs were found to prolong DNA DSB repair in tumor cells. NP HDACIs were also evaluated *in vitro* and *in vivo* in chemoradiotherapy using murine models of colorectal and prostate cancer. NP vorinostat and NP quisinostat demonstrated higher therapeutic efficacy than small molecule HDACIs. Our work demonstrates that NP

formulations of HDACs are promising cancer therapeutics with the potential to significantly improve chemoradiotherapy.

Supplementary Material

Refer to Web version on PubMed Central for supplementary material.

ACKNOWLEDGMENTS

This work was supported by the University Cancer Research Fund from the University of North Carolina and R01CA178748-01 from the National Institutes of Health/National Cancer Institute. AZW was also supported by the National Institutes of Health Center for Nanotechnology Excellence Grant 1-U54-CA151652-01. We also thank the Animal Studies Core at the University of North Carolina for their assistance with procedures in this manuscript.

The authors confirm that there are no known conflicts of interest associated with this publication and there has been no significant financial support for this work that could have influenced its outcome.

REFERENCES

- [1]. Johnstone RW. Histone-deacetylase inhibitors: novel drugs for the treatment of cancer. *Nat Rev Drug Discov.* 2002; 1:287–99. [PubMed: 12120280]
- [2]. Lane AA, Chabner BA. Histone Deacetylase Inhibitors in Cancer Therapy. *Journal of Clinical Oncology.* 2009; 27:5459–68. [PubMed: 19826124]
- [3]. Piekarz RL, Frye R, Turner M, Wright JJ, Allen SL, Kirschbaum MH, et al. Phase II Multi-Institutional Trial of the Histone Deacetylase Inhibitor Romidepsin As Monotherapy for Patients With Cutaneous T-Cell Lymphoma. *Journal of Clinical Oncology.* 2009; 27:5410–7. [PubMed: 19826128]
- [4]. Mann BS, Johnson JR, Cohen MH, Justice R, Pazdur R. FDA Approval Summary: Vorinostat for Treatment of Advanced Primary Cutaneous T-Cell Lymphoma. *The Oncologist.* 2007; 12:1247–52. [PubMed: 17962618]
- [5]. Halperin, E.; Perez, C.; Brady, L. *Perez and Brady's Principles and Practice of Radiation Oncology.* Fifth. Lippincott Williams & Wilkins; Philadelphia, Pa: 2008.
- [6]. Chinnaiyan P, Vallabhaneni G, Armstrong E, Huang SM, Harari PM. Modulation of radiation response by histone deacetylase inhibition. *Int J Radiat Oncol Biol Phys.* 2005; 62:223–9. [PubMed: 15850925]
- [7]. Flatmark K, Nome R, Folkvord S, Bratland A, Rasmussen H, Ellefsen M, et al. Radiosensitization of colorectal carcinoma cell lines by histone deacetylase inhibition. *Radiation Oncology.* 2006; 1:25. [PubMed: 16887021]
- [8]. Chen C-S, Wang Y-C, Yang H-C, Huang P-H, Kulp SK, Yang C-C, et al. Histone Deacetylase Inhibitors Sensitize Prostate Cancer Cells to Agents that Produce DNA Double-Strand Breaks by Targeting Ku70 Acetylation. *Cancer Research.* 2007; 67:5318–27. [PubMed: 17545612]
- [9]. Munshi A, Tanaka T, Hobbs ML, Tucker SL, Richon VM, Meyn RE. Vorinostat, a histone deacetylase inhibitor, enhances the response of human tumor cells to ionizing radiation through prolongation of γ -H2AX foci. *Molecular Cancer Therapeutics.* 2006; 5:1967–74. [PubMed: 16928817]
- [10]. Camphausen K, Burgan W, Cerra M, Oswald KA, Trepel JB, Lee M-J, et al. Enhanced Radiation-Induced Cell Killing and Prolongation of γ H2AX Foci Expression by the Histone Deacetylase Inhibitor MS-275. *Cancer Research.* 2004; 64:316–21. [PubMed: 14729640]
- [11]. Rogakou EP, Pilch DR, Orr AH, Ivanova VS, Bonner WM. DNA Double-stranded Breaks Induce Histone H2AX Phosphorylation on Serine 139. *Journal of Biological Chemistry.* 1998; 273:5858–68. [PubMed: 9488723]
- [12]. Camphausen K, Tofilon PJ. Inhibition of Histone Deacetylation: A Strategy for Tumor Radiosensitization. *Journal of Clinical Oncology.* 2007; 25:4051–6. [PubMed: 17827453]

- [13]. Arts J, King P, Mariën A, Floren W, Beliën A, Janssen L, et al. JNJ-26481585, a Novel “Second-Generation” Oral Histone Deacetylase Inhibitor, Shows Broad-Spectrum Preclinical Antitumoral Activity. *Clinical Cancer Research*. 2009; 15:6841–51. [PubMed: 19861438]
- [14]. Lee JH, Choy ML, Ngo L, Foster SS, Marks PA. Histone deacetylase inhibitor induces DNA damage, which normal but not transformed cells can repair. *Proceedings of the National Academy of Sciences*. 2010; 107:14639–44.
- [15]. Venugopal B, Baird R, Kristeleit RS, Plummer R, Cowan R, Stewart A, et al. A Phase I Study of Quisinostat (JNJ-26481585), an Oral Hydroxamate Histone Deacetylase Inhibitor with Evidence of Target Modulation and Antitumor Activity, in Patients with Advanced Solid Tumors. *Clinical Cancer Research*. 2013; 19:4262–72. [PubMed: 23741066]
- [16]. Fang J, Nakamura H, Maeda H. The EPR effect: Unique features of tumor blood vessels for drug delivery, factors involved, and limitations and augmentation of the effect. *Adv Drug Deliv Rev*. 2011; 63:136–51. [PubMed: 20441782]
- [17]. Pridgen EM, Langer R, Farokhzad OC. Biodegradable, polymeric nanoparticle delivery systems for cancer therapy. *Nanomedicine (Lond)*. 2007; 2:669–80. [PubMed: 17976029]
- [18]. Zhang L, Chan JM, Gu FX, Rhee J-W, Wang AZ, Radovic-Moreno AF, et al. Self-Assembled Lipid–Polymer Hybrid Nanoparticles: A Robust Drug Delivery Platform. *ACS Nano*. 2008; 2:1696–702. [PubMed: 19206374]
- [19]. Makadia HK, Siegel SJ. Poly Lactic-co-Glycolic Acid (PLGA) as Biodegradable Controlled Drug Delivery Carrier. *Polymers*. 2011; 3:1377–97. [PubMed: 22577513]
- [20]. Maeda H, Wu J, Sawa T, Matsumura Y, Hori K. Tumor vascular permeability and the EPR effect in macromolecular therapeutics: a review. *Journal of Controlled Release*. 2000; 65:271–84. [PubMed: 10699287]
- [21]. Ree AH, Dueland S, Folkvord S, Hole KH, Seierstad T, Johansen M, et al. Vorinostat, a histone deacetylase inhibitor, combined with pelvic palliative radiotherapy for gastrointestinal carcinoma: the Pelvic Radiation and Vorinostat (PRAVO) phase 1 study. *The Lancet Oncology*. 2010; 11:459–64. [PubMed: 20378407]
- [22]. Kelly W, O'Connor O, Krug L, Chiao J, Heaney M, Curley T, et al. Phase I study of an oral histone deacetylase inhibitor, suberoylanilide hydroxamic acid, in patients with advanced cancer. *J Clin Oncol*. 2005; 23:3923–31. [PubMed: 15897550]
- [23]. Hrkach J, Von Hoff D, Ali MM, Andrianova E, Auer J, Campbell T, et al. Preclinical Development and Clinical Translation of a PSMA-Targeted Docetaxel Nanoparticle with a Differentiated Pharmacological Profile. *Science Translational Medicine*. 2012; 4:128ra39.

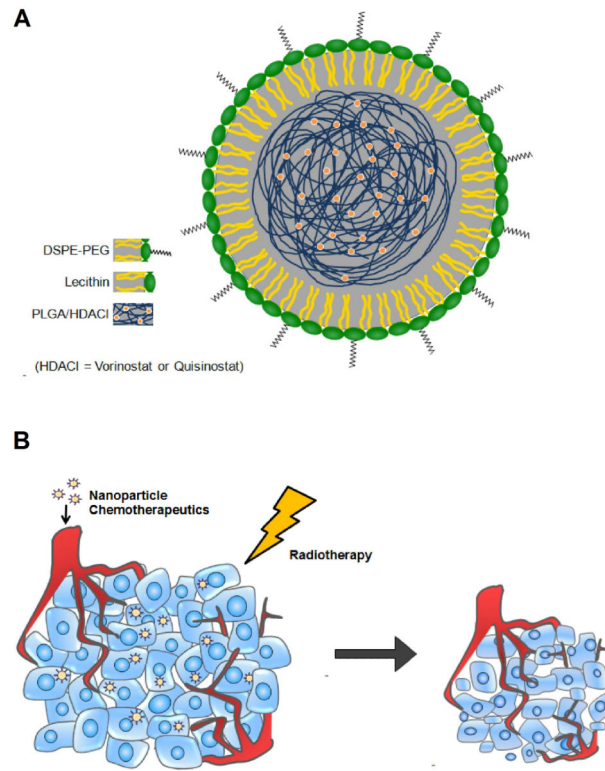


Figure 1. (A) Schematic of NP formulations of HDACIs. (B) NP therapeutics preferentially accumulates in tumors *via* the EPR effect allowing for tumor tissue to receive both the radiosensitizer and radiotherapy.

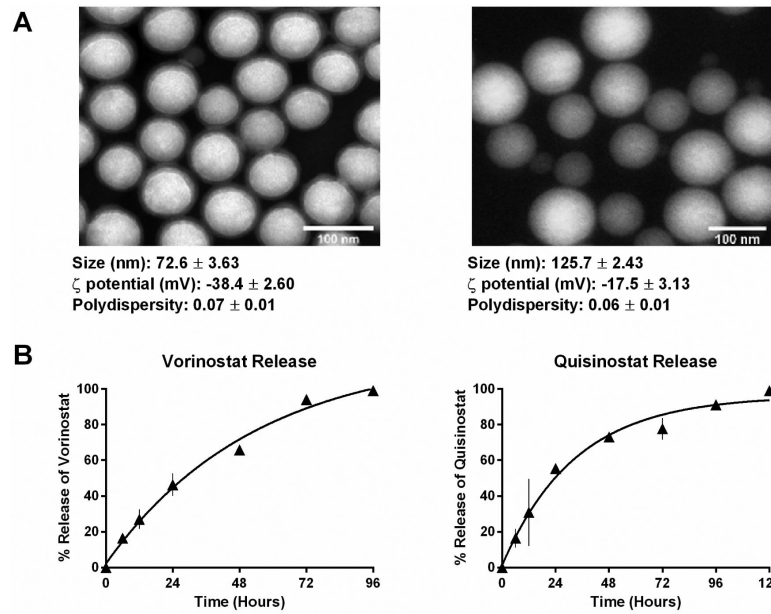
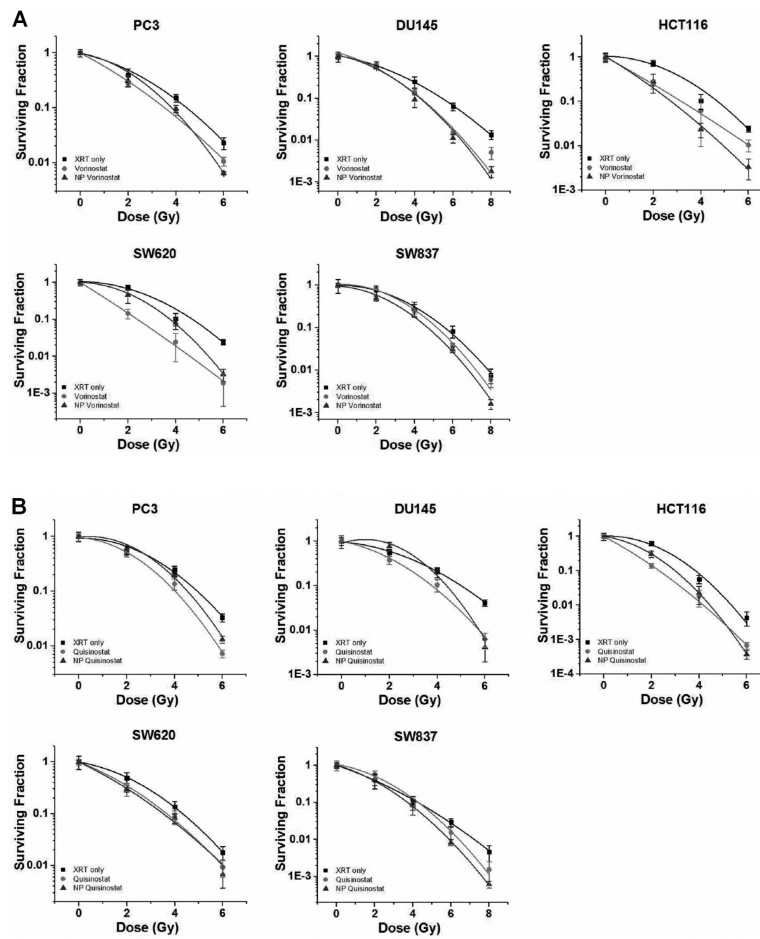


Figure 2. Characterization of NP HDACIs. (A) TEM images of NP vorinostat and NP quisinostat depicting a monodisperse population of particles with a size distribution of 72.6 ± 3.63 and 125.7 ± 2.43 respectively. (B) Drug-release curves of NP vorinostat and NP quisinostat. NP HDACIs releases HDACI in a first-order release kinetics. NP HDACIs were incubated in phosphate buffered saline at 37°C .

**Figure 3.**

Efficacy of NP vorinostat and NP quisinostat as radiosensitizers in PC3, DU145, HCT116, SW620, and SW837 cell lines *in vitro*. Cells were treated with saline, vorinostat, quisinostat, NP vorinostat or NP quisinostat. The cells were then irradiated at different doses (2 Gy, 4 Gy, 6 Gy and 8 Gy). Surviving fractions of the cells were calculated at each radiotherapy dose. Error bars correspond to the standard error of the mean (n=3).

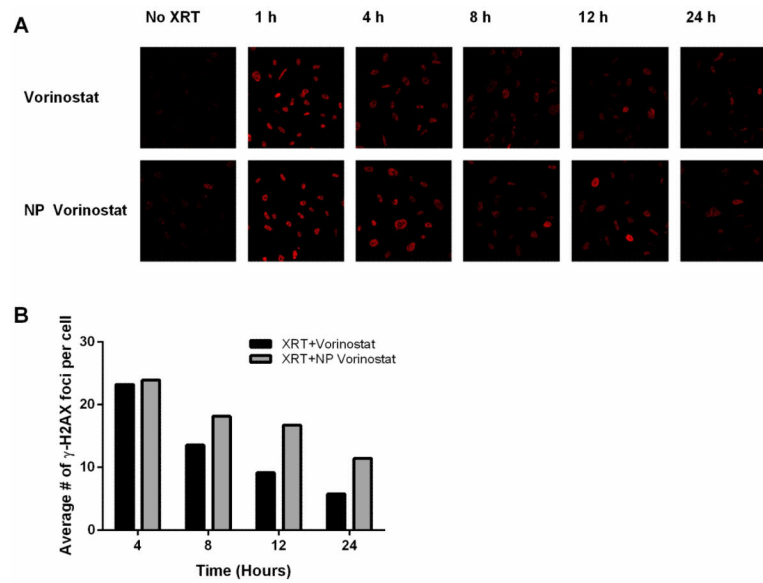


Figure 4.

Influence of vorinostat and NP vorinostat on radiation-induced γ -H2AX foci. PC3 cells were grown in a 24-well plate and then treated with vorinostat or NP vorinostat at 1 μ M small molecule equivalent for 24 h, washed thrice, irradiated (2 Gy), and fixed at the specified times for immunocytochemical analysis of nuclear γ -H2AX foci. **(A)** Micrographs obtained from cells exposed to vorinostat or NP vorinostat. **(B)** Quantitative analysis of foci present in the cells following treatments.

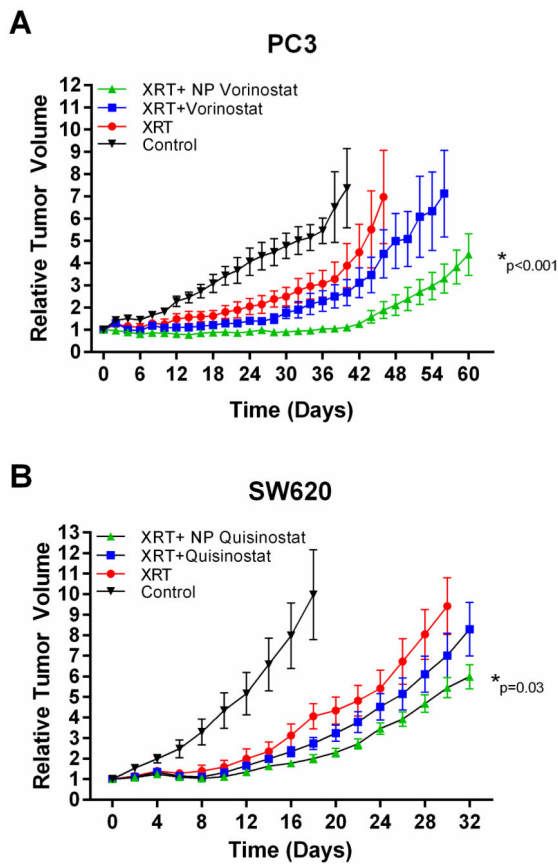


Figure 5.

Efficacy of NP HDACIs as radiosensitizers in chemoradiotherapy for solid tumor cell lines *in vivo*. Mice bearing flank tumor xenografts were administered (intravenous) with saline, vorinostat, NP vorinostat, quisinostat or NP quisinostat followed by radiotherapy. Tumors were irradiated to a total dose of 3 Gy at 3 h after chemotherapy injection. Changes in tumor volume were measured and the tumor growth delay curves for mice bearing PC3 (A) and SW620 (B) tumors were generated.